ADVANCED FUNCTIONAL MATERIALS

FULL PAPER

DOI: 10.1002/adfm.200600215

Band-Offset Engineering for Enhanced Open-Circuit Voltage in Polymer–Oxide Hybrid Solar Cells**

By *Dana C. Olson*, *Sean E. Shaheen*, *Matthew S. White*, *William J. Mitchell*, *Maikel F. A. M. van Hest*, *Reuben T. Collins*, and *David S. Ginley**

The power conversion efficiency of organic and hybrid solar cells is commonly reduced by a low open-circuit voltage (V_{OC}). In these cases, the V_{OC} is significantly less than the energy of the lowest energy absorbed photon, divided by the elementary charge q. The low photovoltage originates from characteristically large band offsets between the electron donor and acceptor species. Here a simple method is reported to systematically tune the band offset in a π-conjugated polymer–metal oxide hybrid donor–acceptor system in order to maximize the V_{OC}. It is demonstrated that substitution of magnesium into a zinc oxide acceptor (ZnMgO) reduces the band offset and results in a substantial increase in the V_{OC} of poly(3-hexylthiophene) (P3HT)–ZnMgO planar devices. The V_{OC} is seen to increase from 500 mV at $x = 0$ up to values in excess of 900 mV for $x = 0.35$. A concomitant increase in overall device efficiency is seen as x is increased from 0 to 0.25, with a maximum power-conversion efficiency of 0.5 % obtained at $x = 0.25$, beyond which the efficiency decreases because of increased series resistance in the device. This work provides a new tool for understanding the role of the donor–acceptor band offset in hybrid photovoltaics and for maximizing the photovoltage and power-conversion efficiency in such devices.

1. Introduction

Photovoltaic researchers are pursuing a variety of approaches directed toward making photovoltaics (PVs) cost effective as a large-scale, renewable energy resource. Solution-based approaches in particular are intrinsically low-cost because of the low temperatures and atmospheric processing conditions required. Ultimately the goal of these approaches is to enable roll-to-roll fabrication on flexible substrates, which would result in low balance-of-system costs for the entire PV module. Polymer-based solar cells have the potential to be a viable pathway to this vision.[1–3]

Organic-based devices can be realized through a number of approaches. One of the most successful to date is the polymer–fullerene blend that has demonstrated a certified power-conversion efficiency of 4.8 %.[4,5] Another promising approach is based on organic–inorganic composites, though to date these hybrid devices have measured efficiencies of less than 2 %.[6–10] Most of these device configurations suffer from reduced V_{OC} because of the large band offset between the electron donor and acceptor materials. Notable exceptions to this are devices based on polymer–polymer blends, which exhibit relatively large V_{OC} (> 1 V) but small short-circuit current (J_{SC}),[11] as well as a report of a hybrid polymer–ZnO device, fabricated using in situ thermal conversion of a ZnO precursor with a V_{OC} of 1.14 V.[6] In order to increase the V_{OC} and efficiency in such devices the donor–acceptor band offset must be optimized. This has been previously demonstrated in polymer–fullerene blend devices, where the electron affinity of the fullerene derivative was modified leading to a change in the V_{OC}.[12] Because of the range of lowest unoccupied molecular orbital (LUMO) levels in the available fullerene derivatives, an increased V_{OC} was not observed. Here, we demonstrate that substitution of Mg into ZnO to form $Zn_{1-x}Mg_xO$ provides continuous control of the band offset over a large range and leads to increased V_{OC} values in hybrid devices using P3HT as the electron donor as apposed to P3HT–fullerene blends.

The V_{OC} in an "excitonic" solar cell is fundamentally determined by the effective electronic bandgap of the donor–acceptor system.[13] This is given by the difference between the thermalized potential energies of the electron in the conduction band or LUMO of the acceptor and the hole in the valence band or highest occupied molecular orbital (HOMO) of the donor, as seen in Figure 1. The actual V_{OC} in a real device will be less than this value because of several factors, including the injected (dark) current, carrier recombination either in the bulk or at the electrodes, or incomplete splitting of the quasi-

[*] Dr. D. S. Ginley, Dr. D. C. Olson, Dr. S. E. Shaheen, M. S. White, Dr. W. J. Mitchell, Dr. M. F. A. M. van Hest
National Renewable Energy Laboratory
Mail Stop 3211, 1617 Cole Blvd. Golden, CO 80401 (USA)
E-mail: david_ginley@nrel.gov
Dr. D. C. Olson, Prof. R. T. Collins
Department of Physics, Colorado School of Mines
Golden, CO 80401 (USA)
M. S. White
Department of Physics, University of Colorado
Boulder, CO 80309 (USA)

[**] The authors gratefully acknowledge Dr. Jorge Piris, Dr. Nikos Kopidakis, and Dr. Garry Rumbles at the NREL for preliminary TRMC measurements. This work was funded under support from the Director's Discretionary Research and Development (DDRD) Fund at the National Renewable Energy Laboratory under the US Department of Energy (DOE) contract DE-AC36-99-GO10337.

ADVANCED FUNCTIONAL MATERIALS

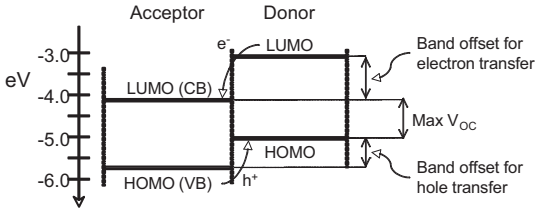

Figure 1. Band diagram of donor–acceptor pair with V_{OC} as determined by band offset. CB: conduction band; VB: valence band.

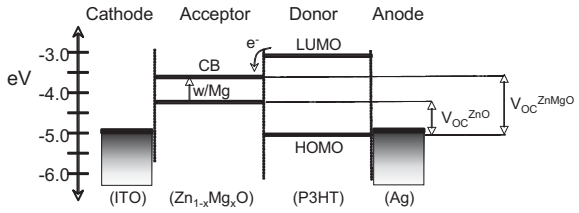

Figure 2. Band diagram of indium tin oxide (ITO)–$Zn_{1-x}Mg_xO$–P3HT–Ag hybrid polymer–metal oxide device.

Fermi levels, as determined by the incident light intensity.[12,14] Additionally, the V_{OC} can be reduced by chemical potential pinning to poorly optimized electrodes,[15] and variation of the work function of either the hole- or electron-collecting electrode has been demonstrated to influence the V_{OC} in polymer PV devices.[12,16,17] Interface dipoles at the electrode can also play an important role in determining the V_{OC}.[18] Interfacial dipoles at the donor–acceptor interface in polymer–polymer devices have been observed to increase the V_{OC}.[19]

That the V_{OC} is directly controlled by the effective electronic bandgap of the donor–acceptor system has been demonstrated in other ways besides the above discussion on the alteration of the fullerene LUMO level. Changes in V_{OC} have also been observed by varying the oxidation potential of the electron-donating polymer.[20] When the oxidation potential was increased in a range of polythiophenes blended with [6,6]-pheny-C_{61} butyric acid methyl ester (PCBM), a corresponding increase in the V_{OC} was observed. These results provide a good indication that the HOMO level in the donor molecule in part determines the V_{OC}. Similar results have been observed for poly(2-methoxy-5-(3′,7′-dimethyloctyloxy)–1,4-phenylenevinylene) (MDMO–PPV) blended with fullerene acceptors with reduced electron affinities indicating that the other major component in determining the V_{OC} is the LUMO level of the electron acceptor.[12] Also, it has been shown that solvation effects can result in an increase in the V_{OC} through changes in morphology in a bulk-heterojunction device.[21] Generally, this is a relatively small effect, where V_{OC} increases with the level of molecular disorder in the film, which is likely due to a shift of the HOMO level of the donor molecule away from vacuum. This can often be seen with an accompanying blue-shift in the absorption spectra.

Underlying the above discussion is the effect of the band offset on the dynamics of the charge-transfer process between the donor and acceptor. It is expected that a larger offset leads to a faster and/or more stable charge transfer, but a precise description is not known. Greater thermal energy may help to drive the carriers away from the interface,[22] which would reduce the recombination rate and increase the photocurrent. The band offset should at least be larger than the exciton binding energy of the donor, but by how much is unclear. Complicating matters has been a lack of donor–acceptor systems in which the band offset is easily tunable over a large, continuous range. This work describes a model donor–acceptor system that demonstrates systematic tuning of the band offset by substitutional doping of Mg into ZnO, which modifies its conduction-band energy. As shown in Figure 2, this leads to a reduction in the band offset and a concomitant increase in the V_{OC} for electron transfer from P3HT to $Zn_{1-x}Mg_xO$ in a bilayer device. We find no reduction, and in fact a small increase, in the photocurrent as x is increased from 0 to 0.25 resulting in the V_{OC} increasing from 500 to 800 mV. This implies that, at least in the regime of band offsets in these devices, the thermal energy of the carriers after charge transfer is not a limiting factor in the production of photocurrent.

Alteration of the bandgap of ZnO has been demonstrated by partial substitution of Zn with a variety of divalent cations. Mg substitution has been shown in pulsed laser deposition (PLD) experiments to increase the bandgap,[23] whereas Cd has been shown to reduce it.[24] These appear to be true solid solution systems showing very small structural changes to the ZnO wurtzite structure. Additionally, the samples can be doped in the conventional fashion with Al, Ga, or In giving rise to the potential for independently controlling the gap and doping level in the metal oxide.[25] Thin films of $Zn_{1-x}Mg_xO$ have been fabricated through a sol–gel deposition method with Mg content up to an x value of 0.36. An increase in the bandgap from 3.40 to 3.93 eV was observed with no phase separation through annealing up to 700 °C.[26] Recent studies have shown that much of that increase should be in the conduction band, which agrees with the common anion rule.[27] Here we find a near-unity correlation between the V_{OC} and the bandgap of the $Zn_{1-x}Mg_xO$ for values of x up to 0.2, beyond which the operation of the device is affected detrimentally by series resistance. This indicates that nearly all of the band-edge movement takes place in the conduction band, as would be expected for an n-type material such as ZnO.

2. Synthesis and Characterization of $Zn_{1-x}Mg_xO$ Films from Solution

The $Zn_{1-x}Mg_xO$ thin films were fabricated by spin-coating from a solution of zinc and magnesium acetates at the proper molar ratio, similar to methods used for nucleation layer films made in previous studies.[10] The resultant zinc–magnesium acetate precursor films were thermally annealed for 5 min at 300 °C in air, and the $Zn_{1-x}Mg_xO$ films were rinsed with deionized water and ethanol. The alloy composition of the film deposited on glass was confirmed by inductively coupled plasma analysis (ICP) with very good agreement to the calculated composition based on the metal content in the original solution. The $Zn_{1-x}Mg_xO$ films deposited on glass were investi-

gated with X-ray diffraction (XRD) to determine the phase and also the maximum Mg content before phase separation occurred. XRD data for the $Zn_{1-x}Mg_xO$ thin films ($0 < x < 0.45$) are shown in Figure 3. With increasing Mg content the films remain in the wurzite-type ZnO phase without any impurity phase until $x = 0.45$ when there is phase separation to include the cubic MgO phase. The maximum Mg content is significantly larger than the thermodynamic limit of $x = 0.04$.[28] Incorporation of Mg into the ZnO phase does decrease the crystallinity of the film, with the (100), (002), and (101) peaks becoming weaker and broadening with increasing Mg content at the low annealing temperatures employed here. No clear shift in the positions of the peaks are observed, indicating that Mg is incorporated without significant strain on the lattice, which would be expected based on the ionic radii of Zn^{2+} and Mg^{2+} (0.60 and 0.57 Å, respectively). The XRD study indicates that for PV devices, phase separation limits usable Mg contents to less than $x = 0.45$. As such, the $x = 0.45$ Mg film is not employed in other measurements mentioned below.

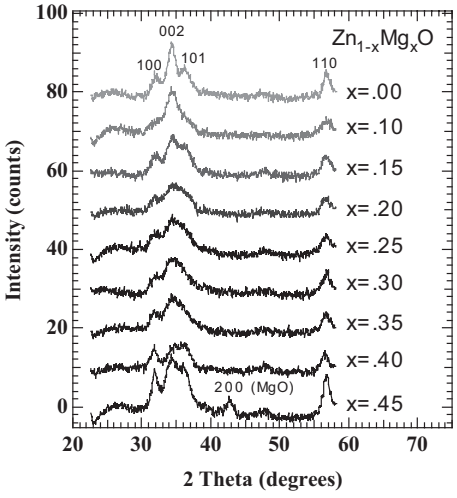

Figure 3. XRD θ–2θ scans for $Zn_{1-x}Mg_xO$ films ($0 < x < 0.45$) deposited on glass.

Absorption spectra of the $Zn_{1-x}Mg_xO$ films ($0 < x < 0.40$) deposited on quartz substrates are seen in Figure 4. It is assumed that the $Zn_{1-x}Mg_xO$ material is a direct-bandgap semiconductor based on its efficient PL, and that ZnO itself is a direct-bandgap semiconductor being developed for UV-LEDs (LED: light-emitting diode).[29,30] All of the samples are transparent in the visible region from 400 to 800 nm, with an absorption edge in the UV region. Optical bandgaps were estimated using the Urbach model[31] by fitting the absorption coefficient α to the equation $\alpha = A^*(h\nu - E_g)^{1/2}$, where A* is a constant related to the refractive index and the electron/hole effective masses. A plot of α^2 versus hν (photon energy) was used to estimate the bandgap of the $Zn_{1-x}Mg_xO$ films. The bandgap increases linearly from 3.2 to 4.0 eV with Mg composition up to $x = 0.40$, as seen in Figure 4, indicating that Mg is effectively incorporated into the ZnO lattice.

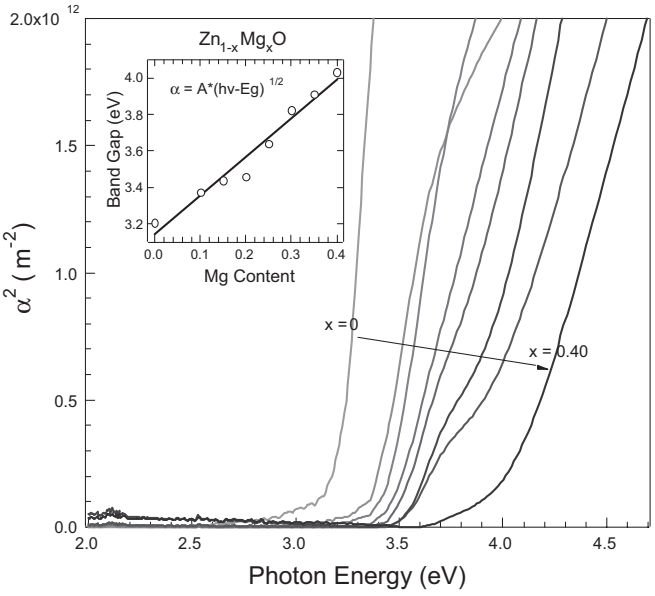

Figure 4. Absorption coefficient (α^2) versus photon energy (hν) for $Zn_{1-x}Mg_xO$ films ($0 < x < 0.40$) deposited on quartz. Inset shows increase in bandgap with Mg composition.

The work function, or the Fermi energy, of the $Zn_{1-x}Mg_xO$ films deposited on indium tin oxide (ITO) was estimated by using Kelvin probe measurements of the surface-potential difference with respect to a stainless-steel reference, measured in an N_2 atmosphere. Since ZnO grown as described here is typically an n-type semiconductor, it is assumed that the Fermi energy will be close to the conduction-band energy. The change in work function with composition gives an estimate for the change in the conduction-band position with Mg content, although here the conduction-band energy cannot be unambiguously extracted from knowledge of the work function since the intrinsic carrier density is too low to be easily measured and also is likely to depend on Mg content. As shown in Figure 5, the work function is seen to decrease with increasing Mg composition for values of x up to 0.25, which indicates a shift in the conduction band closer to vacuum. The work function mea-

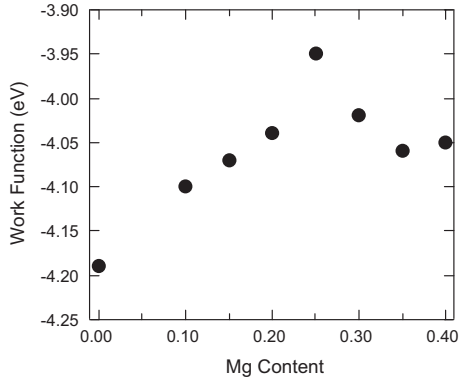

Figure 5. Work function (eV) versus Mg content for $Zn_{1-x}Mg_xO$ films ($0 < x < 0.40$) deposited on ITO.

ADVANCED FUNCTIONAL MATERIALS

sured here for Zn_1Mg_0O is 4.2 eV, which is the same as the accepted value for the conduction band in ZnO. This implies the existence of a high intrinsic carrier density in the film; however, Hall-effect measurements were not sensitive enough to detect the carrier density, giving an upper bound of 10^{16}–10^{17} cm^{-3}. We note that the Kelvin-probe data is highly sensitive to the adsorption of water or hydroxyl ions on the surface of a film that may occur immediately after annealing, and thus this data is useful only in showing the general trend in the movement of the conduction band closer to vacuum with higher Mg content.

3. Increase of V_{OC} with Mg Content in P3HT/$Zn_{1-x}Mg_xO$ Bilayer Devices

To observe the effects of varied band offsets on the V_{OC}, hybrid P3HT–$Zn_{1-x}Mg_xO$ bilayer devices were prepared. Bilayer devices were chosen here to demonstrate the concept, though nanostructured $Zn_{1-x}Mg_xO$ materials will ultimately be required for higher-efficiency devices. The P3HT used for this portion of the study was synthesized in house. The current density–voltage (J–V) curves for the P3HT–$Zn_{1-x}Mg_xO$ bilayer devices are shown in Figure 6. The substitution of Mg into the ZnO acceptor results in a systematic increase in the V_{OC} from 500 mV for $Zn_{1.0}Mg_{0.0}O$ to greater than 900 mV for

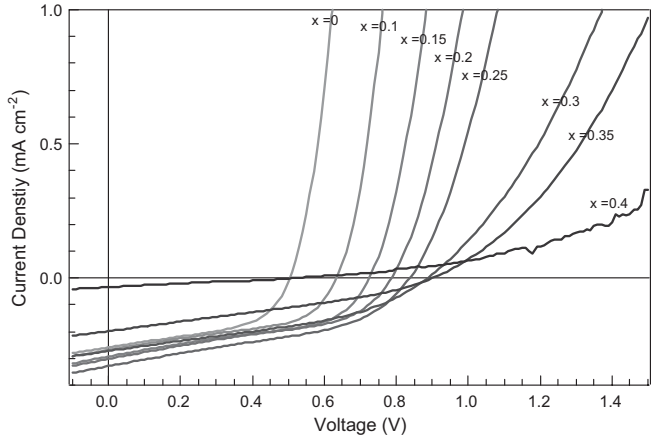

Figure 6. Current density versus voltage for P3HT–$Zn_{1-x}Mg_xO$ devices ($0 < x < 0.40$).

$Zn_{0.65}Mg_{0.35}O$, as seen in Figure 7. When the Mg composition increases to $x = 0.40$ the V_{OC} drops dramatically. Similarly, the J_{SC} and η increase with increasing Mg content, though they begin to fall off above $x = 0.25$, as seen in Figure 7. At these high levels of Mg content the series resistance of the $Zn_{1-x}Mg_xO$ adversely affects the diode performance of the device. As shown in Figure 8, the series resistance increases exponentially from 4.2 to 72 $\Omega\,cm^2$ with increasing Mg content. A constant contribution to the series resistance originating from the rest of the device is evident at low Mg content and is included in the fit equation in Figure 8. This agrees with preliminary time-re-

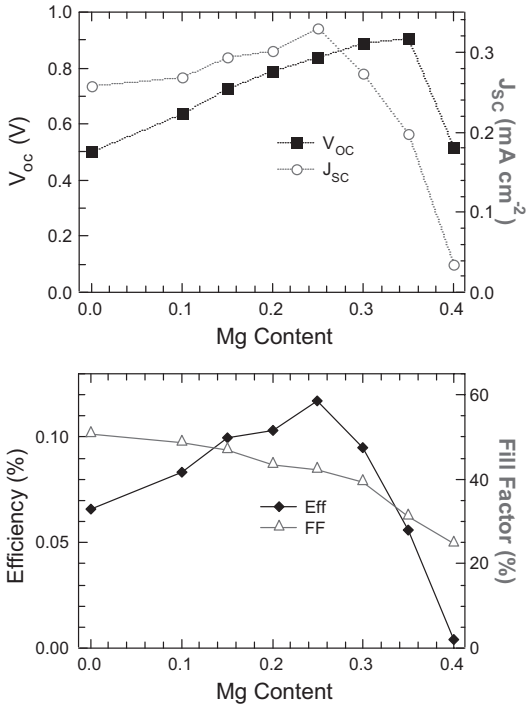

Figure 7. Photovoltaic performance of synthesized P3HT–$Zn_{1-x}Mg_xO$ devices ($0 < x < 0.40$). V_{OC} (■) and J_{SC} (○) versus Mg content (top). Efficiency (◆) and *FF* (△) versus Mg content (bottom).

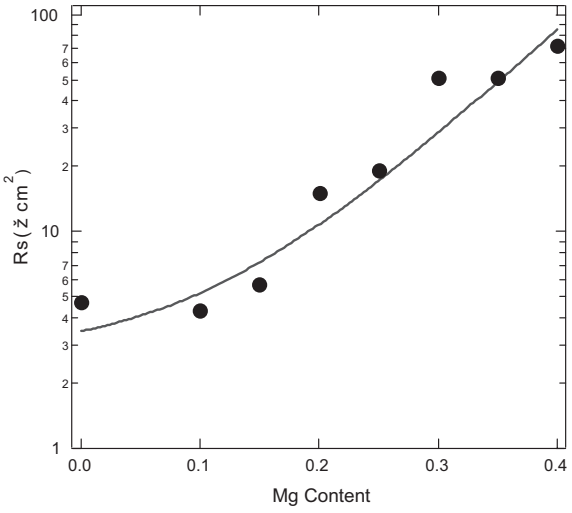

Figure 8. P3HT–$Zn_{1-x}Mg_xO$ bilayer device series resistance versus Mg composition. This fit line corresponds to $Rs = 3.47\ \Omega\,cm^2 + (0.8{*}e^{(11.6{*}Mg\ Content)} - 0.8)\ \Omega\,cm^2$.

solved microwave conductivity (TRMC) data (to be presented elsewhere) on the $Zn_{1-x}Mg_xO$ films, which indicate that increasing Mg content results in an exponential decrease of the mobility by almost two orders of magnitude. The exponent in both cases is approximately the same when fitting with respect to Mg content.

Figure 9 shows the V_{OC} as a function of the optical bandgap of $Zn_{1-x}Mg_xO$. The V_{OC} is observed to increase linearly with a

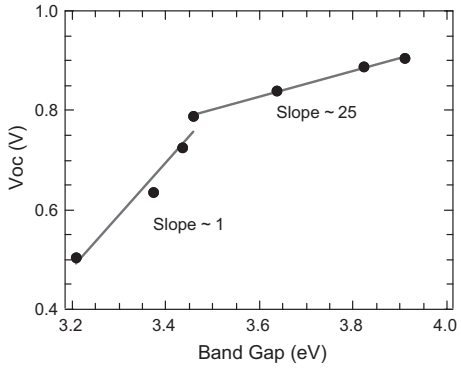

Figure 9. V_{OC} versus $Zn_{1-x}Mg_xO$ bandgap in P3HT–$Zn_{1-x}Mg_xO$ bilayer devices.

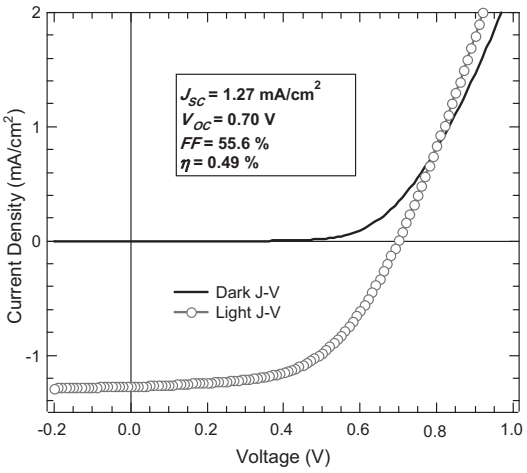

Figure 10. Current density versus voltage of an increased surface roughness $Zn_{75}Mg_{25}O$–Rieke P3HT device. Dark *J–V* (solid line), light *J–V* (○).

slope of ca. 1 for a Mg content up to $Zn_{0.80}Mg_{0.20}O$, above which the slope decreases to 0.25. The increased bandgap of $Zn_{1-x}Mg_xO$ results in a shift in its conduction-band energy closer to vacuum, which corresponds to a decrease in the donor–acceptor band offset and an increase in the V_{OC}, as depicted in Figure 2.

Despite the increase in series resistance with increased Mg content the J_{SC} actually increases by 25 % up to $Zn_{0.75}Mg_{0.25}O$. A likely explanation for this is increased roughness of the $Zn_{1-x}Mg_xO$ surface. Atomic force microscopy measurements revealed an increase in surface roughness as the Mg content was increased, although this was highly dependent on the age of the precursor solution. Solutions that were several weeks old yielded films with an increase in surface roughness of a factor of two between $x = 0$ and 0.25. We attribute this to the formation of nanoparticles as the $Zn_{1-x}Mg_xO$ precursor solution ages, a process that is apparently accelerated as the Mg content is increased. The solutions used for the data presented here were a few days old resulting in a moderate increase in surface roughness at higher Mg content. Regardless of these complications, the finding that the photocurrent does not decrease with decreasing band offset implies that the thermalization energy given to the carriers upon charge transfer is not critical to prevent recombination, at least in the range of band offsets obtained here. Further study is necessary to directly measure the charge-transfer and recombination rates in these hybrid devices.

To verify the observed trend in V_{OC} found above, a second source of P3HT (Rieke Metals) was used for an identical study of the effect of Mg content on device performance. Similar results were observed for the Rieke P3HT as for the in-house-synthesized material, however the J_{SC} values were dramatically higher, and the V_{OC} values were slightly lower for the latter. Also, the series-resistance values were lower and the fill factor (*FF*) values were higher for the Rieke P3HT. The highest-efficiency device for this series of devices was also found at $x = 0.25$. This device exhibited a J_{SC}, V_{OC}, *FF*, and η of 1.27 mA cm^{-2}, 0.70 V, 55.6 %, and 0.49 %, respectively, as shown in Figure 10. We attribute the enhanced *FF* and J_{SC} in the Rieke P3HT to improved molecular ordering of this material, leading to a higher hole mobility. This can be explained by the larger weight-average molecular weight (M_w) resulting from the different synthetic routes used for the Rieke P3HT versus the in-house polymer[32,33] The M_w of the polymers were measured to be 11 000 g mol^{-1} for the in-house P3HT and 49 200 g mol^{-1} for the Rieke P3HT. The mobility of P3HT has been shown to increase substantially with increasing molecular weight.[34,35] This effect has been observed in P3HT–PCBM blend devices as well with higher M_w polymers resulting in increased J_{SC} values.[36] The decreased V_{OC} values in the devices using Rieke P3HT can also be explained by increased ordering that results in a slight decrease in the HOMO–LUMO gap, thus reducing the effective bandgap of the donor–acceptor system and reducing the V_{OC}. Similar results have been observed for polymer–fullerene bulk heterojunction devices[21] and in studies of the structural and optical properties of P3HT thin films and solutions.[37–40]

4. Conclusions

The V_{OC} of hybrid P3HT–ZnO devices was enhanced by systematically increasing the bandgap and position of the conduction band edge through the substitution of Mg into the ZnO crystal structure. As a result of the increased bandgap, the electron affinity of the acceptor was effectively reduced. The substitution of Mg for Zn in ZnO thereby decreases the band offset between the LUMO of the polymer donor and the conduction band of the acceptor metal oxide material. The V_{OC} was increased from 500 to 900 mV in the P3HT–$Zn_{1-x}Mg_xO$ devices through the substitution of Mg into ZnO. This is the highest published V_{OC} to date for P3HT-based devices. The results for the bilayer devices indicate that moving the conduction band of the electron acceptor closer to the vacuum level yields a subsequent increase of the V_{OC}, with no loss in J_{SC}. The ability to easily tune the band offsets in hybrid polymer–$Zn_{1-x}Mg_xO$ devices provides a tool for investigating the fundamental nature of the generation of photovoltage in these devices and provides a pathway to higher device efficiencies.

5. Experimental

Devices were fabricated on patterned ITO-coated glass substrates with a sheet resistance of 13 $\Omega\,cm^{-2}$ that were first cleaned by ultrasonic agitation in acetone and isopropanol each for 10 min followed by a oxygen-plasma treatment of 150 W at 500 mTorr (1 Torr ≈ 133.3 Pa) for 5 min. The $Zn_{1-x}Mg_x$ acetate solutions were prepared using a molar ratio of zinc acetate-2-hydrate and magnesium acetate-4-hydrate ratio as indicated dissolved in a mixture of ethanol amine in 2-methoxyethanol, where the ratio of ethanol amine to total metal acetate was 1.0 and the total concentration of metal acetate was 0.75 M. These solutions were spin-coated onto the ITO, which functions as the transparent electron-collecting electrode. After thermal annealing the zinc acetate film for 5 min at 300 °C in air, the $Zn_{1-x}Mg_xO$ film was rinsed with deionized water and ethanol. The $Zn_{1-x}Mg_xO$ film thickness was measured as 50–80 nm. The films were then dried in air for 20 min at 200 °C. The films were removed from the hotplate and cooled in flowing N_2 gas, and a 200 nm layer of P3HT was spin-coated from a 30 $mg\,mL^{-1}$ chlorobenzene solution on top of this structure. A 90 nm silver top contact was deposited using thermal evaporation through a shadow mask to form the positive back electrode with active areas for each device of 0.1 cm × 0.1 cm. This was followed by another thermal anneal at 120 °C for 10 min in air prior to measurement. Devices were subsequently stored in air in the dark.

All PV characterizations were performed in air without the use of UV filters. Measurements using our user facility Spectrolab XT-10 solar simulator were calibrated for 100 $mW\,cm^{-2}$ of AM1.5 illumination using a reference Si solar cell. The response of the reference cell is periodically calibrated against a P3HT-based organic solar cell that has been submitted to the NREL Measurements and Characterization division for certified measurement and spectral-mismatch correction. Samples under test were loaded into a device holder with a quartz window. The lamp intensity for the XT-10 measurements was set such that the reflection off the top surface of the window, which is approximately 9 %, was taken into account, and the intensity of light incident on the surface of the device was 100 $mW\,cm^{-2}$. *J–V* measurements were taken using a Keithley 238 high-current-source power meter. XRD data were performed on a Bruker D8 with a 2D large-area detector and an *x–y* sample positioning stage. Each sample was measured for 2 h to increase the ratio of signal to noise. Film thicknesses were measured on a Dektak 3 profilometer. ICP measurements were made using a Varian ICP 100. Absorption spectra were recorded on a Hewlett Packard 8453 UV/vis spectrophotometer. Work-function measurements were performed using a McAllister Technical Services KP6500 Kelvin probe under flowing N_2 or air. The P3HT was both synthesized in house and purchased from Rieke Metals and used as received. The synthesized polymer was prepared from 2,5-dibromo-3-hexylthiophene via Grignard metathesis [32]. Purification was carried out by precipitation into methanol followed by soxhlet fractionation using methanol initially and then chloroform. The chloroform fraction was precipitated into methanol to give the desired polymer.

Received: March 6, 2006
Final version: May 18, 2006
Published online: December 13, 2006

[1] S. E. Shaheen, D. S. Ginley, G. E. Jabbour, *MRS Bull.* **2005**, *30*, 10.
[2] C. J. Brabec, N. S. Sariciftci, J. C. Hummelen, *Adv. Funct. Mater.* **2001**, *11*, 15.
[3] K. M. Coakley, M. D. McGehee, *Chem. Mater.* **2004**, *16*, 4533.
[4] C. J. Brabec, M. Koppe, M. Morana, D. Muehlbacher, C. Waldauf, P. Denk, M. C. Scharber, presented at the SPIE Annual Meeting, San Diego, CA, **2005**.
[5] G. Li, V. Shrotriya, J. Huang, Y. Yao, T. Moriarty, K. Emery, Y. Yang, *Nat. Mater.* **2005**, *4*, 864.
[6] W. J. E. Beek, L. H. Slooff, M. M. Wienk, J. M. Kroon, R. A. J. Janssen, *Adv. Funct. Mater.* **2005**, *15*, 1703.
[7] W. J. E. Beek, M. M. Wienk, R. A. J. Janssen, *Adv. Mater.* **2004**, *16*, 1009.
[8] W. J. E. Beek, M. M. Wienk, M. Kemerink, X. Yang, R. A. J. Janssen, *J. Phys. Chem. B* **2005**, *109*, 9505.
[9] K. M. Coakley, M. D. McGehee, *Appl. Phys. Lett.* **2003**, *83*, 3380.
[10] D. C. Olson, J. Piris, R. T. Collins, S. E. Shaheen, D. S. Ginley, *Thin Solid Films* **2006**, *496*, 26.
[11] M. M. Koetse, J. Sweelssen, K. T. Hoekerd, H. F. M. Schoo, S. C. Veenstra, J. M. Kroon, X. Yang, J. Loos, *Appl. Phys. Lett.* **2006**, *88*, 083 504.
[12] C. J. Brabec, A. Cravino, D. Meissner, N. S. Sariciftci, T. Fromherz, M. T. Rispens, L. Sanchez, J. C. Hummelen, *Adv. Funct. Mater.* **2001**, *11*, 374.
[13] B. A. Gregg, *MRS Bull.* **2005**, *30*, 20.
[14] B. A. Gregg, M. C. Hanna, *J. Appl. Phys.* **2003**, *93*, 3605.
[15] C. M. Heller, I. H. Campbell, D. L. Smith, N. N. Barashkov, J. P. Ferraris, *J. Appl. Phys.* **1997**, *81*, 3227.
[16] H. Frohne, S. E. Shaheen, C. J. Brabec, D. C. Müller, N. S. Sariciftci, K. Meerholz, *ChemPhysChem* **2002**, *3*, 795.
[17] V. D. Mihailetchi, P. W. M. Blom, J. C. Hummelen, M. T. Rispens, *J. Appl. Phys.* **2003**, *94*, 6849.
[18] V. D. Mihailetchi, L. J. A. Koster, P. W. M. Blom, *Appl. Phys. Lett.* **2004**, *85*, 970.
[19] C. M. Ramsdale, A. C. Arias, J. D. MacKenzie, R. H. Friend, N. C. Greenham, in *2002 MRS Spring Meeting* (Eds: G. E. Jabbour, S. A. Carter, J. Kido, S.-T. Lee, N. S. Sariciftci), Mater. Res. Soc., Warrendale, PA **2002**, pp. 179–190.
[20] A. Gadisa, M. Svensson, M. R. Andersson, O. Inganäs, *Appl. Phys. Lett.* **2004**, *84*, 1609.
[21] J. Liu, Y. Shi, Y. Yang, *Adv. Funct. Mater.* **2001**, *11*, 420.
[22] V. I. Arkhipov, E. V. Emelianova, H. Bässler, *Phys. Rev. Lett.* **1999**, *82*, 1321.
[23] A. Ohtomo, M. Kawasaki, T. Koida, K. Masubuchi, H. Koinuma, Y. Sakurai, Y. Yoshida, T. Yasuda, Y. Segawa, *Appl. Phys. Lett.* **1998**, *72*, 2466.
[24] L. Chen, Z. Ye, D. Ma, B. Zhao, C. Ling, L. Zhu, *J. Cryst. Growth* **2005**, *274*, 458.
[25] K. Matsubara, H. Tampo, H. Shibata, A. Yamada, P. Fons, K. Iwata, S. Niki, *Appl. Phys. Lett.* **2004**, *85*, 1374.
[26] D. Zhao, Y. Liu, D. Shen, Y. Lu, J. Zhang, X. Fan, *J. Appl. Phys.* **2001**, *90*, 5561.
[27] G. V. Rao, F. Säuberlich, A. Klein, *Appl. Phys. Lett.* **2005**, *87*, 032 101.
[28] X. Zhang, X. M. Li, T. L. Chen, J. M. Bian, C. Y. Zhang, *Thin Solid Films* **2005**, *492*, 248.
[29] W. Y. Liang, A. D. Yoffe, *Phys. Rev. Lett.* **1968**, *20*, 59.
[30] W. I. Park, G.-C. Yi, *Adv. Mater.* **2004**, *16*, 87.
[31] J. I. Pankove, *Optical Processes in Semiconductors*, Dover Publications, New York **1971**.
[32] R. S. Loewe, S. M. Khersonsky, R. D. McCullough, *Adv. Mater.* **1999**, *11*, 250.
[33] T.-A. Chen, X. Wu, R. D. Rieke, *J. Am. Chem. Soc.* **1995**, *117*, 233.
[34] C. Goh, R. J. Kline, M. D. McGehee, E. N. Kadnikova, J. M. J. Fréchet, *Appl. Phys. Lett.* **2005**, *86*, 122 110.
[35] R. J. Kline, M. D. McGehee, E. N. Kadnikova, J. Liu, J. M. J. Fréchet, *Adv. Mater.* **2003**, *15*, 1519.
[36] P. Schilinsky, U. Asawapirom, U. Scherf, M. Biele, C. J. Brabec, *Chem. Mater.* **2005**, *17*, 2175.
[37] O. Inganäs, W. R. Salaneck, J.-E. Österholm, J. Laakso, *Synth. Met.* **1988**, *22*, 395.
[38] W. R. Salaneck, O. Inganäs, B. Thémans, J. O. Nilsson, B. Sjögren, *J. Chem. Phys.* **1988**, *89*, 4613.
[39] C. Yang, F. P. Orfino, S. Holdcroft, *Macromolecules* **1996**, *29*, 6510.
[40] M. Trznadel, A. Pron, M. Zagorska, R. Chrzaszcz, J. Pielichowski, *Macromolecules* **1998**, *31*, 5051.